Mechanical Systems and Signal Processing 86 (2017) 40–57

Contents lists available at ScienceDirect

Mechanical Systems and Signal Processing

journal homepage: www.elsevier.com/locate/ymssp

Method of assessing the state of a rolling bearing based on the relative compensation distance of multiple-domain features and locally linear embedding

Shouqiang Kang[a,c,*,1], Danyang Ma[a], Yujing Wang[a,b,*], Chaofeng Lan[a], Qingguo Chen[a], V.I. Mikulovich[c]

[a] School of Electrical and Electronic Engineering, Harbin University of Science and Technology, No. 52, Xuefu Rd, Harbin 150080, PR China

[b] School of Electronics and Information Engineering, Harbin Institute of Technology, No. 92, West Dazhi Street, Harbin 150001, PR China

[c] Radiophysics and Electronics Department, Belarusian State University, Minsk 220030, Belarus

ARTICLE INFO

Keywords:
Ensemble empirical mode decomposition
Multiple-domain features
Locally linear embedding
Relative compensation distance
Performance degradation assessment

ABSTRACT

To effectively assess different fault locations and different degrees of performance degradation of a rolling bearing with a unified assessment index, a novel state assessment method based on the relative compensation distance of multiple-domain features and locally linear embedding is proposed. First, for a single-sample signal, time-domain and frequency-domain indexes can be calculated for the original vibration signal and each sensitive intrinsic mode function obtained by improved ensemble empirical mode decomposition, and the singular values of the sensitive intrinsic mode function matrix can be extracted by singular value decomposition to construct a high-dimensional hybrid-domain feature vector. Second, a feature matrix can be constructed by arranging each feature vector of multiple samples, the dimensions of each row vector of the feature matrix can be reduced by the locally linear embedding algorithm, and the compensation distance of each fault state of the rolling bearing can be calculated using the support vector machine. Finally, the relative distance between different fault locations and different degrees of performance degradation and the normal-state optimal classification surface can be compensated, and on the basis of the proposed relative compensation distance, the assessment model can be constructed and an assessment curve drawn. Experimental results show that the proposed method can effectively assess different fault locations and different degrees of performance degradation of the rolling bearing under certain conditions.

1. Introduction

The running state of a rolling bearing, as one of the most widely used and vulnerable parts of rotating machinery, directly affects the reliability of the operation of the machinery as a whole. The breaking down of a bearing can result in huge economic losses and even casualties [1,2]. Previous research has mostly concentrated on diagnosing and locating a fault. However, the running state of a rolling bearing changes continuously, gradually declining from initial degradation to complete failure. It is thus important to

* Corresponding authors at: School of Electrical and Electronic Engineering, Harbin University of Science and Technology, No. 52, Xuefu Rd, Harbin 150080, PR China.

E-mail addresses: kangshouqiang@163.com (S. Kang), mirrorwyj@163.com (Y. Wang).

[1] Postal address: 445#, School of Electrical and Electronic Engineering, Harbin University of Science and Technology, No.52, Xuefu Road, Nangang District, Harbin 150080, Heilongjiang Province, PR China.

http://dx.doi.org/10.1016/j.ymssp.2016.10.006
Received 28 January 2016; Received in revised form 28 May 2016; Accepted 1 October 2016
Available online 10 October 2016
0888-3270/

Nomenclature

x_{rms}	root mean square
$x_{p\sim p}$	peak-to-peak amplitude
S_f	shape factor
C_f	crest factor
I_f	impulse factor
CL_f	clearance factor
K_v	kurtosis value
F_C	centroid frequency
F_{MS}	mean-square frequency
F_{RMS}	RMS frequency
F_V	frequency variance
H	the number of spectrum lines
s_i	high-dimensional feature vector
S_{Nj}	high-dimensional feature matrix
r	coefficient correlation
$\boldsymbol{z}_i$	the sample point in high-dimensional space
$\boldsymbol{x}_i$	the sample point in low-dimensional space
y_i	classification label
w	weight matrix
C	the penalty parameter of SVM
b	the bias coefficient of SVM
α_i	Lagrange multiplier
$K(,)$	kernel function
s	kernel parameter
d_R	relative distance
d_C	compensation distance
d_{RCD}	relative compensation distance
d	the reduced dimension number
K	the number of neighboring points
F	classification precision
n	the number of samples, a sample is a segment time sequence of the vibration signal
m	the number of sensitive IMFs
q	the polynomial order

Greek symbols

$\alpha_{i,\mathrm{O},t}$	time-domain feature
$\boldsymbol{\alpha}_{i,\mathrm{O}}$	time-domain feature vector comprised of $\alpha_{i,\mathrm{O},t}$
$\beta_{i,\mathrm{O},t}$	frequency-domain feature
$\boldsymbol{\beta}_{i,\mathrm{O}}$	frequency-domain feature vector comprised of $\beta_{i,\mathrm{O},t}$
$\alpha_{i,j,t}$	time-frequency feature: time-domain statistical features of the jth IMF
$\boldsymbol{\alpha}_{i,j}$	time-frequency feature vector comprised of $\alpha_{i,j,t}$
$\beta_{i,j,t}$	time-frequency feature: frequency-domain statistical features of the jth IMF
$\boldsymbol{\beta}_{i,j}$	time-frequency feature vector comprised of $\beta_{i,j,t}$
$\gamma_{i,m}$	time-frequency feature: singular value
$\boldsymbol{\gamma}_i$	singular value feature vector of comprised $\gamma_{i,m}$
ξ_i	non-negative slack variables
$\phi(\boldsymbol{x})$	the mapping function in SVM
$\boldsymbol{\omega}$	the normal vector of the hyperplane in SVM

Subscripts

i, j, k, l	positive integers
N_l	N_l is the number of bearing samples whose state is l
t	positive integers (from 1 to 7)
f	positive integers (from 1 to 16)

establish a unified assessment index with which to effectively assess the fault location and the degree of performance degradation. The aim is to realize active maintenance of a rolling bearing through intelligent quantitative assessment, shifting from scheduled or unscheduled maintenance to condition maintenance.

Performance degradation analysis and predictive maintenance methods for mechanical systems have received attention from researchers at home and abroad. A series of intelligent diagnosis and state assessment methods based on the neural network, Weibull distribution, hidden Markov model, and Gauss mixture model (GMM) have been proposed for performance degradation. Empirical mode decomposition (EMD) has been combined with an artificial neural network to realize the fault diagnosis of a bearing [3]. Deep neural networks have been used to mine the rolling bearing fault characteristics [4], and this method also has been used to intelligently classify the fault states. Weibull distribution parameters have been combined with a simplified fuzzy adaptive resonance theory map to predict the residual life of a rolling bearing [5], and this method can be effectively applied to other rotary machinery. The ratio of adjacent singular values has been calculated to construct feature vectors, which have been combined with the hidden Markov model to realize fault diagnosis and performance degradation assessment of a bearing [6]. The matrix $\boldsymbol{S}$ with time-encoded signal processing and recognition as an original feature vector has been calculated, the number of dimensions has been reduced by employing principal component analysis, and the result subsequently combined with the GMM to assess bearing performance degradation [7]. A fuzzy rule has been introduced to a wavelet filter, and the sum of amplitudes of bearing characteristic frequencies and their harmonics has been used as a performance degradation index to realize early fault diagnosis [8]. A second-generation wavelet has been used to extract wavelet packet energy, features extracted employing Fisher discrimination analysis, and the dispersion of the fuzzy c-mean calculated as an index of performance degradation assessment [9].

Among the above methods of assessing the performance degradation of a rolling bearing, there is a need to extract features and to construct a corresponding assessment index. The intelligent assessment of different fault locations and degrees of performance degradation at the same time requires a method of feature extraction, intelligent classification and state assessment.

In recent years, time-domain and frequency-domain statistical features have been widely used in the extraction of vibration signal features for a rolling bearing [10]. Statistical averages in a single time or frequency domain only reflect global information and not local information in the time and frequency domains, and they are not deemed as effective in fault diagnosis and assessment. A series of time-frequency analysis methods, such as the windowed Fourier transform [11], Wigner–Ville distribution [12], and wavelet analysis [13], have thus been proposed. Time-frequency localization has been introduced to the above methods, but problems remain; e.g., it is difficult to determine the window length and to select the basis function. EMD is characterized by

approximate orthogonality, completion, adaptivity (an adaptive basis function, filtering character and resolution) and mode function component modulation, and is thus suitable for non-stationary signal processing [14]. To restrain the mode confusion phenomenon in EMD, Wu and Huang proposed ensemble empirical mode decomposition (EEMD) [15]. The decomposition results of EEMD depend on two parameters, the ensemble average number and the amplitude of the added noise. Wu and Huang only gave the relationship between the two parameters; generally, these two parameters need to be set by experience, but there is a lack of adaptability to different signals. An energy standard deviation rule has been proposed to add Gaussian white noise in the EEMD method, achieving better performance in terms of restraining the mode confusion and reducing computational costs [16]. Generally, among the intrinsic mode function (IMF) components obtained by EEMD, only a portion contain fault information and are sensitive to the fault. It is thus necessary to establish a method that not only selects the IMF that is effective and sensitive to the fault but also eliminates the component of interference noise or the pseudo component that is independent of the fault. The normalized coefficient of the correlation between the original signal and each IMF has been calculated by setting the threshold with which to select a sensitive IMF at 1/10 of the maximum correlation coefficient [17,18]. As a nonlinear filtering method, singular value decomposition (SVD) highlights the localization character and effectively extracts the periodic component in the original signal to obtain relatively pure fault information [19].

To obtain features of a rolling-bearing vibration signal that are more complete and effective, the multiple-domain feature has been gradually adopted as an effective measure of describing the fault state of a rolling bearing. However, the number of dimensions of the multiple-domain feature is too high. To eliminate correlation and redundancy among the high-dimensional features that characterize the running state of the bearing and to greatly shorten the time required for diagnosis and the construction of the model in the assessment process, it is important to fuse dimensions of the multiple-domain feature and thus reduce their number in the fault diagnosis process. A locality preserving projection (LPP) algorithm has been combined with the GMM to assess the performance degradation of a rolling bearing [20]. The isometric feature mapping reduction technique and support vector machine (SVM) have been used to predict the residual life of a rolling bearing [21]. Fault characteristics have been extracted using detrended fluctuation and rescaled range analyses, which with principal component analysis combined with a neural network to diagnose a fault, provide excellent results [22]. The number of dimensions of high-dimensional fault data has been reduced with supervised locally linear embedding (LLE) projection, obviously improving the efficiency and correctness of diagnosis [23]. The number of dimensions of a band signal that was obtained by wavelet packet decomposition was reduced with an LLE algorithm, improving the classification precision of different fault degrees [24].

In the realization of the accurate assessment of the fault state of a rolling bearing, the selection of an intelligent classification method and the construction of a state assessment model has been the focus of study. The neural network, GMM, and fuzzy clustering analysis each has its advantages, but it is difficult to meet the demand of the sample size in the diagnosis of the rolling-bearing fault. The SVM provides a new way to solve the bottleneck problem in the development of intelligent fault diagnosis, which is restricted by the lack of a large number of fault data samples [25]. However, the application in the fault classification of a rolling bearing mostly concentrates on the identification of different fault locations, which can only judge the affiliation of the bearing fault state and cannot quantitatively describe the fault degree. According to the prior data available, existing intelligent assessment models can be divided into two categories: assessment models based on normal-state data and assessment models based on

Table 1
The feature parameters.

Time-domain feature parameters	Frequency-domain feature parameters	
$x_{rms} = \sqrt{\frac{1}{N}\sum_{n=1}^{N} x^2(n)}$	$F_C = \frac{\sum_{n=1}^{N} \overline{x}(n)x(n)}{2\pi\sum_{n=1}^{N} x(n)^2}$	$p_5 = \frac{\sum_{k=1}^{H} f_k s(k)}{\sum_{k=1}^{H} s(k)}$
$x_{p-p} = x_{\max} - x_{\min}$	$F_{MS} = \frac{\sum_{n=1}^{N} \overline{x}(n)^2}{4\pi^2\sum_{n=1}^{N} x(n)^2}$	$p_6 = \sqrt{\frac{\sum_{k=1}^{H}(f_k - p_5)^2 s(k)}{H}}$
$S_f = \frac{x_{rms}}{\left\lvert\frac{1}{N}\sum_{n=1}^{N} x(n)\right\rvert}$	$F_{RMS} = \sqrt{F_{MS}}$	$p_7 = \sqrt{\frac{\sum_{k=1}^{H} f_k^2 s(k)}{\sum_{k=1}^{H} s(k)}}$
$C_f = \frac{x_{\max}}{x_{rms}}$	$F_V = F_{MS} - (F_C)^2$	$p_8 = \sqrt{\frac{\sum_{k=1}^{H} f_k^4 s(k)}{\sum_{k=1}^{H} f_k^2 s(k)}}$
$I_f = \frac{x_{\max}}{\left\lvert\frac{1}{N}\sum_{n=1}^{N} x(n)\right\rvert}$	$p_1 = \frac{\sum_{k=1}^{H} s(k)}{H}$	$p_9 = \frac{\sum_{k=1}^{H} f_k^2 s(k)}{\sqrt{\sum_{k=1}^{H} s(k)\sum_{k=1}^{H} f_k^4 s(k)}}$
$CL_f = \frac{x_{\max}}{\left\lvert\frac{1}{N}\sum_{n=1}^{N}\sqrt{\lvert x(n)\rvert}\right\rvert^2}$	$p_2 = \frac{\sum_{k=1}^{H}(s(k) - p_1)^2}{H-1}$	$p_{10} = \frac{p_6}{p_5}$
$K_v = \frac{\frac{1}{N}\sum_{n=1}^{N} x^4(n)}{x_{rms}^4}$	$p_3 = \frac{\sum_{k=1}^{H}(s(k) - p_1)^3}{H(\sqrt{p_2})^3}$	$p_{11} = \frac{\sum_{k=1}^{H}(f_k - p_5)^3 s(k)}{H p_6^3}$
where $x(n)$ is a signal series for n = 1,2,...,N, N is the number of data points.	$p_4 = \frac{\sum_{k=1}^{H}(s(k) - p_1)^4}{H(p_2)^2}$	$p_{12} = \frac{\sum_{k=1}^{H}(f_k - p_5)^4 s(k)}{H F_6^4}$
	where $s(k)$ is a spectrum for k = 1,2,...,H, H is the number of spectrum lines: f_k is the frequency value of the kth spectrum line.	

multiple-state data. The former assessment method only refers to typical data in a normal state, and the lack of prior knowledge must affect the assessment precision. The latter can make full use of the prior knowledge to obtain a more accurate result. Obviously, if there is a need to study more than two kinds of state assessment model, multiple-state classifiers must be used, which places a higher demand on the research of the assessment index for performance degradation. Therefore, focusing on the vibration signal of different fault locations and different performance degradation degrees, there is an urgent need to combine an intelligent classifier with a rolling-bearing structure, acceleration sensor positions and the propagation mechanism of vibration, to construct a unified assessment index based on a multiple-state assessment model.

It is difficult to construct a unified failure model because of the complicated working conditions and various fault types [26]. In the assessment of the performance degradation of a bearing, the characteristic parameters will gradually depart from the characteristic distribution of the normal state in a prescribed orbit, and therefore some kind of generalized distance that is calculated using state feature vectors in the process of performance degradation can be used to describe the degree of performance degradation. Generally, rolling bearings comprise an outer ring, inner ring and several rolling elements distributed between the outer and inner rings, and the three components of the bearing affect each other through vibration. To acquire signals of bearing vibration, sensors are often attached to the bearing seat, and are not directly in contact with the fault location. Hence there may be differences (i.e., losses) between the actual fault signal and the vibration signal that is sampled by sensors. Therefore, an assessment method based on the relative compensation distance is proposed for the special structure of the bearing. The relative compensation distance remedies the vibration propagation losses relating to the sensor positions.

The present paper employs EEMD and SVD to extract features of the time–frequency features, where time- and frequency-domain features are combined to construct high-dimensional feature sets in a multiple domain, to eliminate correlation and redundancy among the high-dimensional features and to reduce the number of dimensions of feature sets, according to the special structure of the bearing and the mechanism of vibration propagation between the fault point and sensors. A novel method of assessing the rolling-bearing state based on the relative compensation distance is thus proposed. This method not only improves the precision of fault diagnosis but also effectively assesses the fault location and the degree of performance degradation with a unified assessment index at the same time. The monotonicity and consistency of the performance degradation index and fault degree are well verified with actual vibration data for a bearing.

2. Multiple-domain feature extraction

A feature parameter of a rolling-bearing vibration signal usually only reflects information of a single equipment fault—a kind of fault location or fault state—and a single feature parameter thus cannot completely describe the fault state of the bearing. To use efficiently various statistical features from notable category differences in the time-domain, frequency-domain and time–frequency features, the present paper introduces hybrid-domain feature parameters defined on multiple domains to describe the state of the rolling bearing.

2.1. Time-domain feature parameters

Seven time-domain feature parameters—namely the root mean square (RMS), recorded as x_{rms}, peak-to-peak amplitude $x_{p\sim p}$, shape factor S_f, crest factor C_f, impulse factor I_f, clearance factor CL_f, and kurtosis value K_v —are selected as time-domain features that reflect the fault state of the rolling bearing [10], and the calculation formulas are shown in Table 1. These parameters constitute feature vectors:

$$\boldsymbol{\alpha}_{i,0} = [\alpha_{i,0,1}, \alpha_{i,0,2}, \ldots, \alpha_{i,0,t}], \tag{1}$$

where i=1,...,n, with n being the number of samples, a sample being a segment time sequence of the vibration signal, and t the number of time-domain features (t=7).

2.2. Frequency-domain feature parameters

When a rolling-bearing fault occurs, the energies of different frequency components in the vibration signal change. Therefore, to obtain more complete fault information, 16 frequency-domain feature parameters [10,27]—7YPERLINK /centroid frequency F_C, mean-square frequency F_{MS}, RMS frequency F_{RMS}, frequency variance F_V, and frequency indexes p_1~p_{12}, and the calculation formulas are shown in Table 1. The feature vectors constructed from the frequency features of the original vibration signal are

$$\boldsymbol{\beta}_{i,0} = [\beta_{i,0,1}, \beta_{i,0,2}, \ldots, \beta_{i,0,f}], \tag{2}$$

where i=1,...,n, with n being the number of samples and f the number of frequency-domain features (f =16).

2.3. Time–frequency feature parameters and multi-domain feature vector construction

On the basis of the original signal feature extractions in the time and frequency domains, an improved EEMD decomposition method [16] is used to decompose the vibration signal. Because the IMFs obtained using improved EEMD still contain false components, only some contain information of the rolling-bearing fault. Therefore, the correlation coefficient is used to select the sensitive IMFs. The specific steps are as follows.

Step (1): Decompose the vibration signal of the rolling bearing with the improved EEMD to obtain all IMF components.

Step (2): Normalize all IMF components and the original vibration signal using Eq. (3), and calculate the normalized coefficient of correlation r_j (j=1,...,J) between J IMFs and the original vibration signal:

$$c_{norm} = (c - \bar{c})/std\,(c). \tag{3}$$

In Eq. (3), c represents the IMF component or original vibration signal, $\bar{c}$ is the mean of c, $std\,(c)$ is the standard deviation of c, and c_{norm} is the normalized result of c.

Step (3): Set the threshold as 1/10 of the correlation coefficient to select the IMFs that contain major information about the state of the rolling bearing. If r_j is greater than 1/10 of the correlation coefficient, the jth IMF is retained, and otherwise the jth IMF is eliminated. Using this threshold, all sensitive IMFs are obtained.

The time- and frequency-domain features of each sensitive IMF are displayed as vectors, Eqs. (4) and (5). The matrix is constructed by regarding sensitive IMFs as row vectors, then the matrix is decomposed using SVD and the singular values can be obtained, the vector formed by the singular values is shown as Eq. (6).

$$\boldsymbol{\alpha}_{i,j} = [\alpha_{i,j,1}, \alpha_{i,j,2}, \ldots, \alpha_{i,j,t}], \tag{4}$$

$$\boldsymbol{\beta}_{i,j} = [\beta_{i,j,1}, \beta_{i,j,2}, \ldots, \beta_{i,j,f}], \tag{5}$$

$$\boldsymbol{\gamma}_i = [\gamma_{i,1}, \gamma_{i,2}, \ldots, \gamma_{i,m}], \tag{6}$$

where i=1,...,n, with n being the number of samples, and j=1,...,m, with m being the number of sensitive IMFs that were obtained using the correlation coefficient. t is the number of time-domain features (t=7) and f is the number of frequency-domain features (f =16). $\boldsymbol{\alpha}_{i,j}$ is the jth sensitive IMF time-domain feature of the ith sample, $\boldsymbol{\beta}_{i,j}$ is the jth sensitive IMF frequency-domain feature of the ith sample, and $\boldsymbol{\gamma}_i$ is the feature vector that formed by the singular values obtained by decomposing the sensitive IMF matrix of the ith sample through SVD. Eqs. (4)–(6) are the features based on time-frequency analysis, and are referred to as the time–frequency features.

The time-domain features of the original vibration signal and sensitive IMFs, frequency-domain features of the original vibration signal and sensitive IMFs, and SVD feature values of the sensitive IMF matrix are placed in order of priority. The largest number of sensitive IMFs of different samples is m. When the number of sensitive IMFs is smaller than m, the sensitive IMF matrix is filled with zero vectors to construct high-dimensional feature vectors of the ith sample:

$$\mathbf{s}_i = [\boldsymbol{\alpha}_{i,0}, \boldsymbol{\alpha}_{i,1}, \boldsymbol{\alpha}_{i,2}, \ldots, \boldsymbol{\alpha}_{i,m}, \boldsymbol{\beta}_{i,0}, \boldsymbol{\beta}_{i,1}, \boldsymbol{\beta}_{i,2}, \cdots, \boldsymbol{\beta}_{i,m}, \boldsymbol{\gamma}_i]^{\mathrm{T}}. \tag{7}$$

The feature matrix of each state of the rolling bearing is then constructed using Eq. (7) and denoted

$$\mathbf{S}_{N_l} = [\mathbf{s}_1, \mathbf{s}_2, \ldots, \mathbf{s}_{N_l}]^{\mathrm{T}}, \tag{8}$$

where N_l is the number of bearing samples in state l.

3. Fundamental theory

3.1. Locally linear embedding algorithm

An LLE algorithm is a nonlinear dimension reduction algorithm that employs the local linearity to approximate the global nonlinearity. The main concern is to maintain the local relational order between the data points in the embedding space and the intrinsic space. Each sample point in the space can be expressed by a weighted mean of the points in its neighborhood. The weighted values of all points form a weight matrix in the high-dimensional space, which provides the description of the data points in the low-dimensional space.

The specific algorithm steps are as follows.

Step (1): For each sample point $\boldsymbol{z}_i$ in high-dimensional space, calculate the distance between the sample and the other points, and find the nearest k points to $\boldsymbol{z}_i$. The equation for calculating the distance between two points is

$$d_{ij} = \|\mathbf{z}_i - \mathbf{z}_j\|. \tag{9}$$

Step (2): Calculate the local reconstructed weight matrix of each sample point. The current sample point is expressed by the k nearest neighboring points, and to get the weight matrix, the error function is defined as

$$\varepsilon(\mathbf{w}) = \sum_{i=1}^{n} \left| \mathbf{z}_i - \sum_{j=1}^{k} \mathbf{w}_{ij}\mathbf{z}_j \right|^2. \tag{10}$$

In Eq. (10), if $\boldsymbol{z}_j$ is not the neighboring sample point of $\boldsymbol{z}_i$, then $\mathbf{w}_{ij} = \mathbf{0}$, where $\sum_{j=1}^{k} \mathbf{w}_{ij} = 1$.

Step (3): According to the weight $\boldsymbol{w}_{ij}$ for the sample point $\boldsymbol{z}_i$ and neighboring point $\boldsymbol{z}_j$ in the high-dimensional space, the sample point $\boldsymbol{x}_i$ and neighboring point $\boldsymbol{x}_j$ in low-dimension embedding space can be calculated. The weight is fixed to minimize the loss function

$$\phi(\mathbf{x}) = \sum_{i=1}^{n} \left| \mathbf{x}_i - \sum_{j=1}^{k} \mathbf{w}_{ij}\mathbf{x}_j \right|^2 . \tag{11}$$

By minimizing the loss function to get the corresponding weight matrix and reconstructed coordinates, the data can be processed using the obtained weight matrix to reduce the number of dimensions.

3.2. SVM

The SVM is a machine learning method based on statistical learning theory. The basic concept is to map the training samples from the input space to a higher-dimensional feature space via map function ϕ. Suppose there is a given training sample set $G=\{(\boldsymbol{x}_i, y_i), i=1, 2,..., l\}$, where each sample $x_i \in R^d$ belongs to a class y∈{+1, −1}. When the training data are not linearly divisible in the feature space, the target function can be expressed as

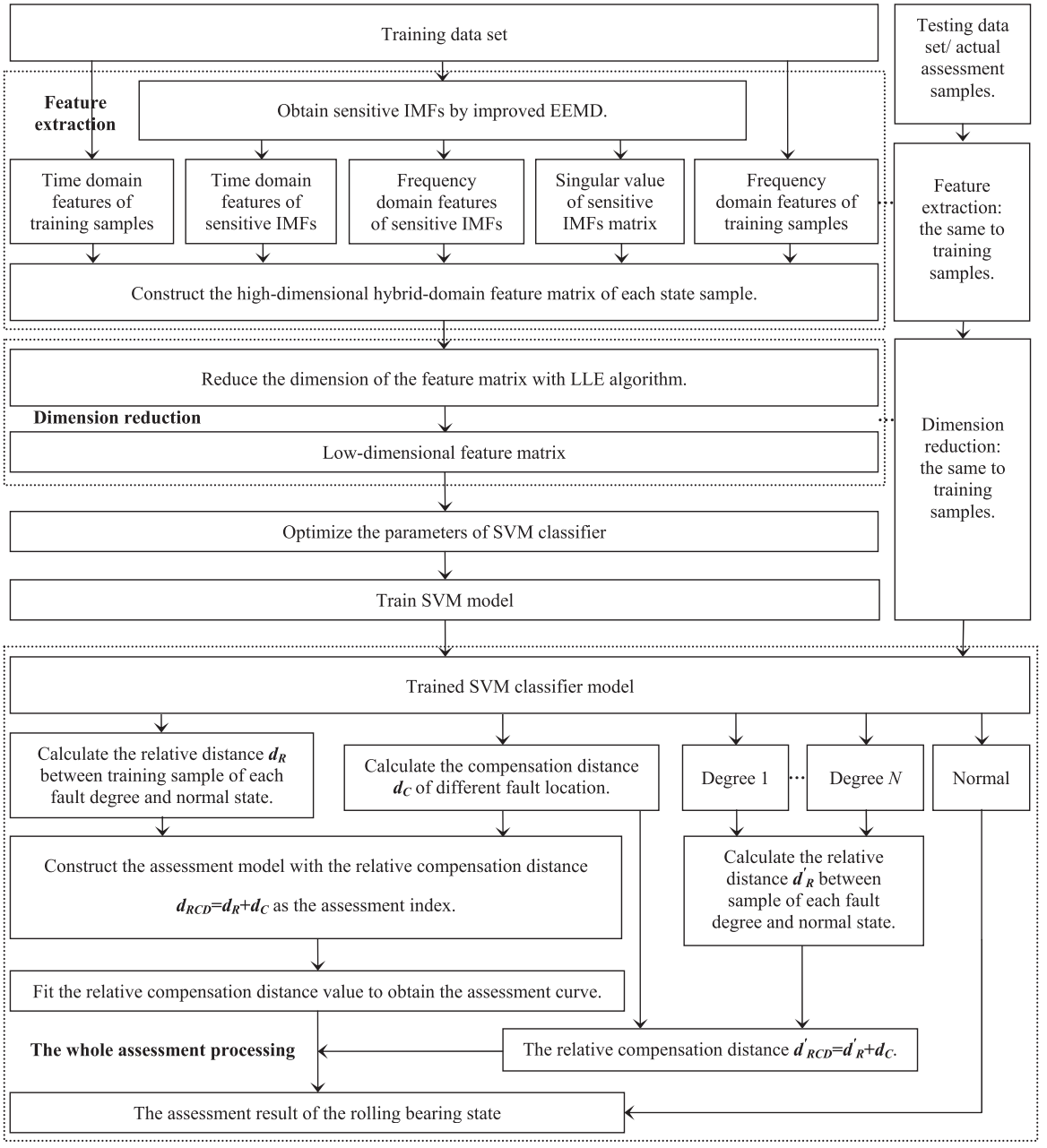

Fig. 1. Flow chart of the assessment of the rolling-bearing fault.

$$\begin{cases} \min \phi(\boldsymbol{\omega}) = \frac{1}{2}\langle \boldsymbol{\omega}\cdot\boldsymbol{\omega}\rangle + C\sum_{i=1}^{l} \xi_i \\ s.\ t \quad y_i(\langle \boldsymbol{\omega}\cdot\phi(\mathbf{x}_i)\rangle + b) \geq 1 - \xi_i, \quad \xi_i \geq 0,\ i = \{1, 2, \ldots, l\}. \end{cases}, \tag{12}$$

where $\boldsymbol{\omega}$ is the normal vector of the hyperplane, C is the penalty parameter, b is the bias coefficient, ξ_i denotes non-negative slack variables, and $\phi(\boldsymbol{x})$ is the mapping function.

By introducing a set of Lagrange multipliers, and using a kernel function to convert the nonlinear problem into a linearly divisible problem, the optimization problem can be rewritten as

$$max: L(\boldsymbol{\omega}, b, \alpha) = \sum_{i=1}^{l} \alpha_i - \frac{1}{2}\sum_{i,j=1}^{l} \alpha_i \alpha_j y_i y_j K(\mathbf{x}_i, \mathbf{x}_j), \tag{13}$$

where $\boldsymbol{\alpha_i}$ is a Lagrange multiplier and $K(,)$ is a kernel function.

Subject to $0 \leq \alpha_i \leq C$, where $\sum_{i=1}^{l} \alpha_i y_i = 0$, the decision function can be obtained as

$$f(\mathbf{x}) = \operatorname{sgn}\left(\sum_{i=1}^{l} \alpha_i y_i K(\mathbf{x}_i, \mathbf{x}) + b\right). \tag{14}$$

The most common kernel function is the radial basis kernel function given by

$$K(\mathbf{x}_i, \mathbf{x}_j) = \exp\left(-\frac{\|\mathbf{x}_i - \mathbf{x}_j\|^2}{2s^2}\right), \tag{15}$$

where s is the kernel parameter.

4. Method of assessing the state of the rolling bearing

To accurately assess the performance degradation state of the rolling bearing, it is important to construct an appropriate assessment model. The assessment model directly affects the assessment results.

4.1. SVM

The optimal classification surface function can be calculated after training the data in the SVM:

$$\boldsymbol{\omega}\cdot\mathbf{x} + b = 0. \tag{16}$$

Supposing that $\boldsymbol{x}_0$ is the feature vector of a sample, then, according to the equation for the distance from the point in air to the plane, the distance between any sample point and the corresponding optimal classification surface in the SVM can be calculated as

$$D = \frac{|\boldsymbol{\omega}\cdot\mathbf{x}_0 + b|}{\|\boldsymbol{\omega}\|}. \tag{17}$$

When the SVM works with multiple classifications, the optimal classification surface between each performance degradation state and normal state is different, but the distance between different performance degradation states and the normal-state optimal classification surface still reflects the relative positions of the normal and fault states. Therefore, the distance between different performance degradation states and the normal state optimal classification surface is called the 'relative distance', denoted $d_{\boldsymbol{R}}$. In Eq. (17), $\boldsymbol{\omega}$ and b can be determined according to different bearing states, and the corresponding relative distance $d_{\boldsymbol{R}}$ can then be calculated.

Because of the special structure of rolling bearing and the sensor positions, there is a kind of degradation relation for different fault locations. The rolling bearing is composed of three compact parts from the inside to outside, namely the inner ring, rolling elements and outer ring.

Sensors are often attached to the bearing seat in the acquisition of the vibration signal of the rolling bearing, not directly in contact with the fault location, the outer ring, inner ring and rolling elements affect each other through vibration, and there must therefore be losses in signal acquisition. When a fault occurs at the outer ring, the vibration signal can be sampled directly by sensors. In contrast, when a fault occurs at a rolling element or the inner ring, the vibration signal will be sampled via the outer ring and rolling elements by the sensors. In these cases, there must be differences (i.e., losses) between the actual fault signal and the vibration signal that was sampled by the sensors. Compensation for the losses is conducive for further analysis. According to the special structure of the rolling bearing, fault location and vibration transmission mechanism, the relative distance between the normal state and the same fault degree in the inner ring, rolling elements and outer ring is digressive. Therefore, when the fault state is assessed according to the relative distance of different fault locations, the corresponding compensation distance must ensure the monotonicity and consistency of the assessment index. According to the above analysis, the compensation scheme is set as

$$\begin{cases} d_{C-IR} = d_{IR-B} + d_{IR-OR} + d_{B-OR} \\ d_{C-B} = d_{B-OR} \\ d_{C-OR} = 0 \end{cases}, \tag{18}$$

where $d_{IR\text{-}B}$ is the relative distance between the inner ring and rolling element, $d_{IR\text{-}OR}$ is the relative distance between the inner

ring and outer ring, and $d_{B\text{-}OR}$ is the relative distance between the rolling element and outer ring. $d_{C\text{-}IR}$ is the compensation distance of the inner ring, $d_{C\text{-}B}$ is the compensation distance of the rolling element, and $d_{C\text{-}OR}$ is the compensation distance of the outer ring; $d_{C\text{-}IR}$, $d_{C\text{-}B}$ and $d_{C\text{-}OR}$ are all referred to as the compensation distance, denoted d_C. The outer ring is wrapped with a bearing seat and is closest to the sensors, and the compensation distance of the outer ring is thus zero.

The result of the relative distance between the bearing performance degradation state and normal state plus the corresponding compensation distance is called the 'relative compensation distance' d_{RCD}, denoted $d_{RCD} = d_R + d_C$.

The above definition of the relative compensation distance is chosen as an assessment index with which to assess the fault location and degree of performance degradation of the rolling bearing. The relative distance between sample points of each fault degree and normal samples is calculated, and the corresponding compensation distance is then added according to the compensation scheme, and the performance degradation assessment curve of the rolling bearing is fitted according to the performance degradation assessment model, in preparation for the following performance degradation assessment.

4.2. Assessment of the state of the rolling bearing

Fig. 1 is a flow chart of the assessment of the fault state of the rolling bearing.

The specific steps for the assessment of the performance degradation of the rolling bearing based on Fig. 1 are as follows.

Step (1): Feature extraction. Extract the time- and frequency-domain features of each vibration signal state of the rolling bearing, decompose the vibration signal with improved EEMD, select sensitive IMFs using the correlation coefficient, calculate the time- and frequency-domain features of sensitive IMFs, and decompose the sensitive IMF matrix employing SVD to obtain a singular value. Finally, construct a high-dimensional hybrid-domain feature matrix that describes the running state of the rolling bearing.

Step (2): Feature reduction. Reduce the number of dimensions of each state feature matrix using the LLE algorithm and eliminate the redundancy of high-dimensional features to get the low-dimensional feature matrix.

Step (3): Distance calculation. Input the low-dimensional feature vectors that are the reduced training samples to the trained SVM classification model. Calculate the relative distance between different fault locations and different fault degrees and the normal state, and calculate the compensation distance of each fault location at the same time.

Step (4): Construction of the assessment model. Use the relative distance between the rolling-bearing performance degradation state and normal state plus the corresponding compensation distance, denoted d_{RCD}=d_R+d_C, to construct the assessment model. Then fit the relative compensation distance to obtain the performance degradation assessment curve.

Step (5): Performance degradation assessment. Repeat steps (1) and (2) for testing or assessment samples to obtain low-dimensional feature vectors, and input them into the trained SVM classification model to identify the fault state of testing or assessment samples; i.e., the normal or fault state. In the case of the normal state, continue to run the equipment and conclude that the assessment result is normal. In the case of the fault state, determine the location and degree of the fault for the sample using the trained SVM classification model in step (3), and obtain the corresponding compensation distance. Calculate the relative distance between this fault state and the normal-state optimal classification surface $d_R^{'}$, plus its corresponding compensation distance $d_C^{'}$. The result is the corresponding relative compensation distance $d_{RCD}^{'}$. Then this value can be located on the assessment curve. From this curve, it is straightforward to find the fault location and performance degradation.

5. Practical analysis

Experimental data for a rolling bearing were obtained from the electric engineering laboratory of Case Western Reserve University [28]. The bearing type is a deep-groove ball bearing SKF6205. Acceleration sensors were arranged on the bearing seat at the driving end and fan end of the motor, the vibration signal was acquired with a 16-channel data logger, and the signal sampling frequency was set at 48 kHz. The bearing test stand is shown in Fig. 2.

Experiments were conducted under different load and speed conditions for four states: the normal state and states with a fault in the inner ring, rolling element or outer ring. For each fault location, there were three degrees of fault: a damage diameter of 7 mil (referred to as fault degree 1), 14 mil (referred to as fault degree 2), or 21 mil (referred to as fault degree 3).

In the present study, a sampling frequency of 48 kHz was set for the vibration signal at the drive end of the rolling bearing. So, we

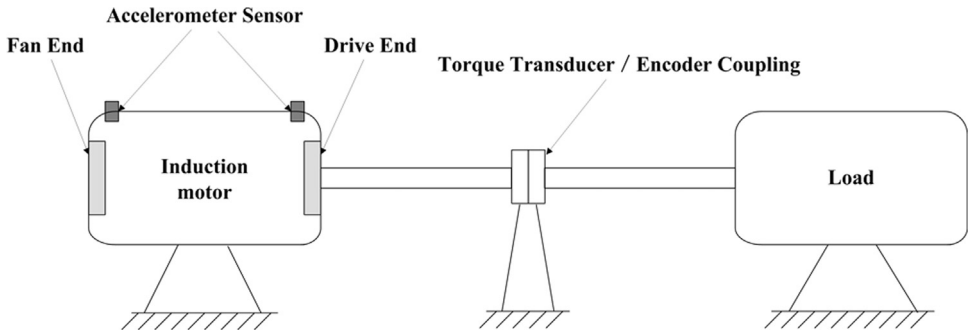

Fig. 2. Schematic diagram of the test stand.

Table 2
Description of bearing data sets.

Data set	Load (hp)	RPM	The number of samples	Fault type	Fault diameter (mil)
A/B/C/D/E	0/1/2/3/0-3	1797/1772/1750/1730/ (the above four speed)	50/65/80/65/225	N	0
			50/65/80/65/225	B	7
			50/65/80/65/225	B	14
			50/65/80/65/225	B	21
			50/65/80/65/225	IR	7
			50/65/80/65/225	IR	14
			50/65/80/65/225	IR	21
			50/65/80/65/225	OR	7
			50/65/80/65/225	OR	14
			50/65/80/65/225	OR	21

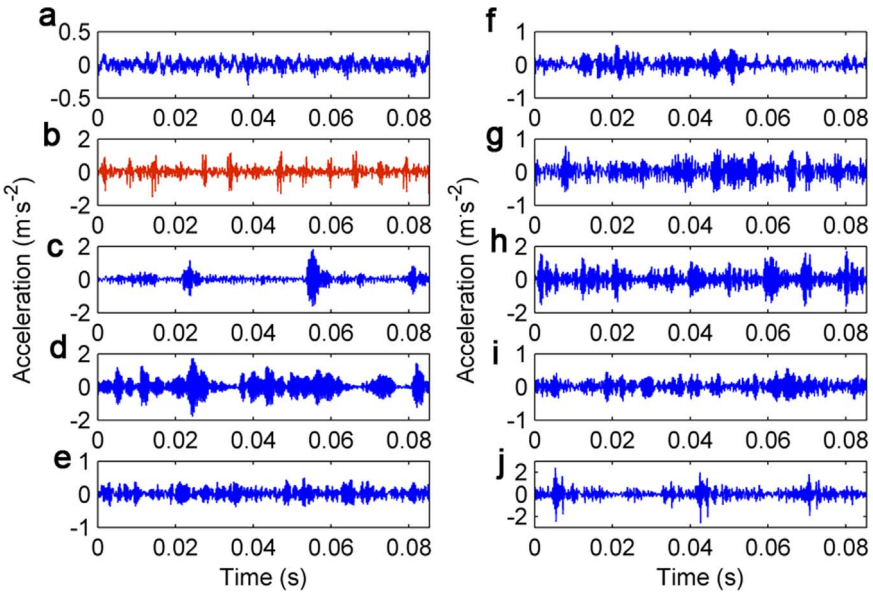

Fig. 3. Time-domain waveforms of the rolling-bearing vibration for 10 conditions: (a) normal, (b) IR07, (c) IR14, (d) IR21, (e) B07, (f) B14, (g) B21, (h) OR07, (i) OR14, (j) OR21.

have defined data sets A, B, C, D, and E, which contain different loads and different rotational speeds. The data of each data set are shown in Table 2. Data set A comprises 500 data samples that cover four fault conditions (normal condition, outer ring fault, rolling elements and inner ring fault) under a 0 hp load and 1797 rpm. Each fault condition includes three fault degrees; specifically, we have damage diameter 7 mil (recorded as fault degree 1), 14 mil (recorded as fault degree 2) and 21 mil (recorded as fault degree 3). The composition of data sets B, C, and D are similar to data set A. Data set E comprises 2250 data samples that cover four fault conditions and four loads, and each fault condition includes three fault degrees. IR07, IR14 and IR21 respectively denote signals for fault degrees 1, 2 and 3 of the inner ring, B07, B14 and B21 respectively denote signals for fault degrees 1, 2 and 3 of the rolling element, and OR07, OR14 and OR21 respectively denote signals for fault degrees 1, 2 and 3 of the outer ring. Shown in Fig. 3 are the time-domain vibration waveforms for ten different types of conditions, for example, the decomposition of the inner-ring fault degree 1 (IR07) using the improved EEMD and setting the expectation error to 1%. According to the energy standard deviation, the ensemble average number can be calculated and is 361. The decomposition results are shown in Fig. 4.

Experiments were performed with the adoption of two schemes. **Experiment scheme 1** (the experiment scheme of the original manuscript) was designed based on data set E; a third of each state samples were randomly selected as training data sets to construct both the SVM classification and assessment models, and the remaining two-thirds were used as testing data sets of both models.

Experiment scheme 2 was designed based on data sets A, B, C, and D, all of data sets A (load 0 hp, speed 1797 rpm) and C (load 2 hp, speed 1750 rpm) were used as the training data sets for the SVM classification and assessment models. Data sets B (load 1 hp, speed 1772 rpm) and D (load 3 hp, speed 1730 rpm) were used as testing data sets for both models.

Experiment 1: Comparison of feature reduction algorithms.

(1) Comparison of the performance of feature reduction.

Based on the data set of experiment scheme 1, the experimental data consist of the vibration signal for the normal state and three different fault locations (inner ring, rolling element and outer ring), with each state having four loads. Multiple-domain features of each vibration signal, including seven time-domain features, were extracted, and feature vectors were constructed following Eq. (1).

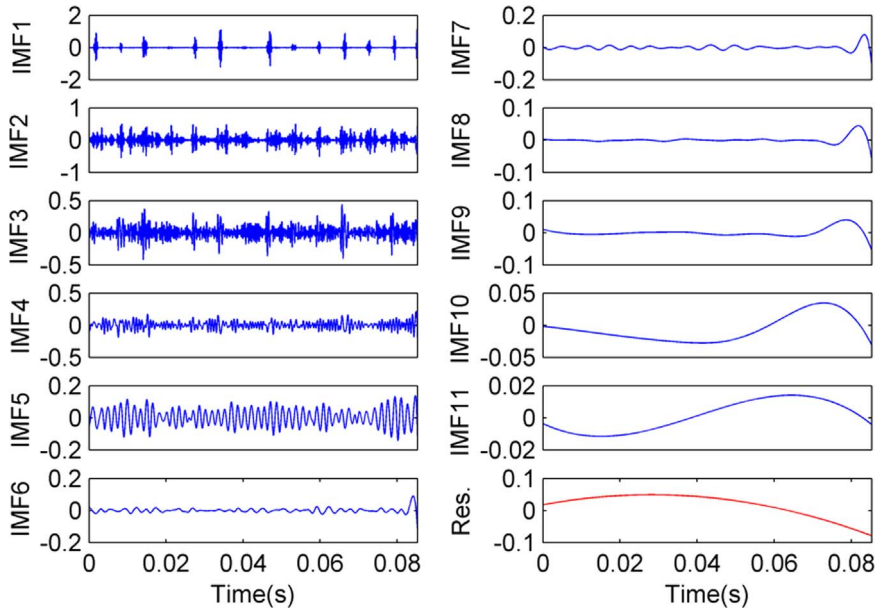

Fig. 4. Decomposition results of IR07 obtained with improved EEMD.

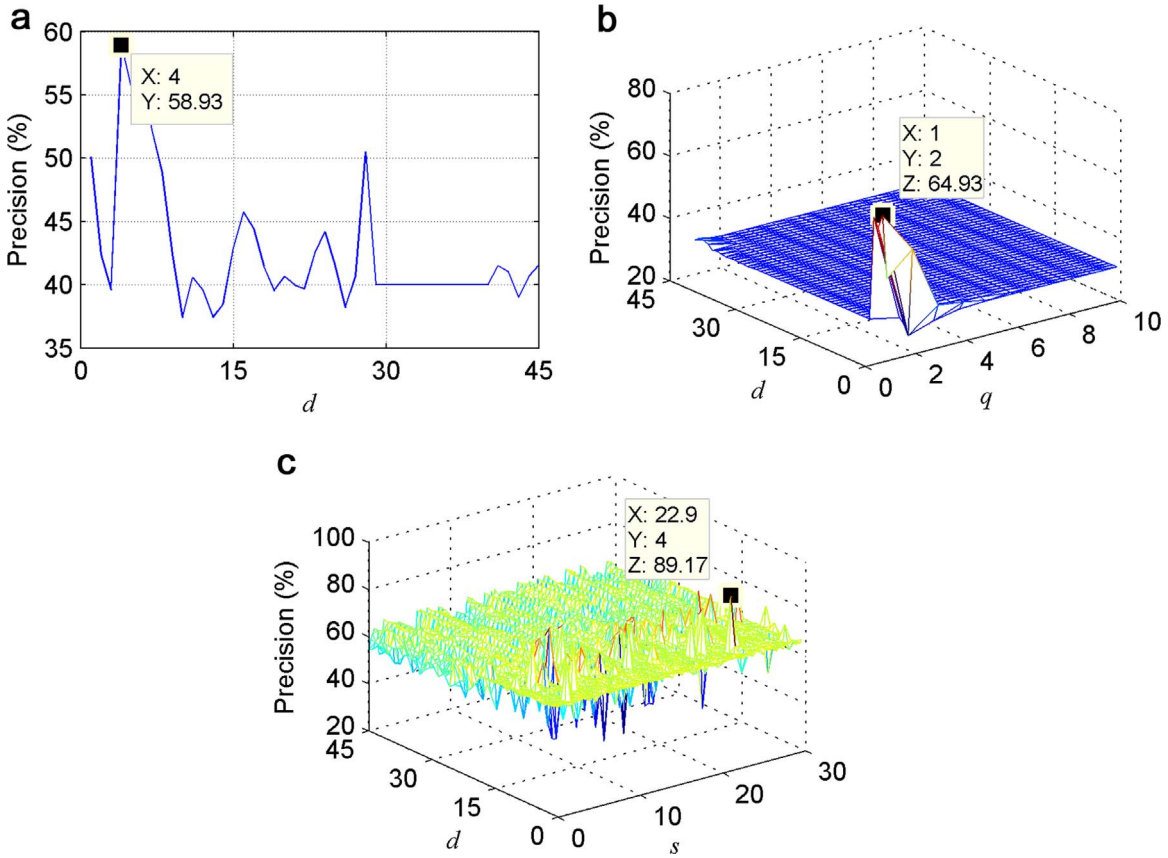

Fig. 5. The relations between the recognition precision and the parameters of KPCA: (a) Linear kernel function (b) Polynomial kernel function, and (c) Radial basis kernel function.

Sixteen frequency-domain features were extracted, and feature vectors were constructed following Eq. (2). Also the time–frequency features were extracted using the improved EEMD. The time–frequency features consist of time- and frequency-domain features of the sensitive IMFs and the singular value of the sensitive IMF matrix, with the feature vectors of Eqs. (4)–(6) constructed previously.

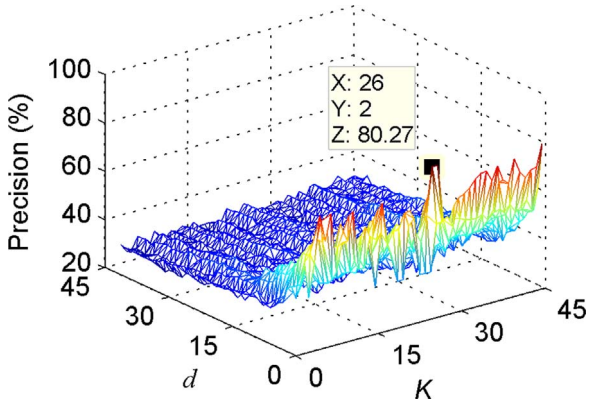

Fig. 6. Relations between the recognition precision and parameters d and K for LPP.

Feature vectors were constructed from features of the time domain, frequency domain and all the time–frequency features of each vibration signal following Eq. (7). For several vibration signal features of each state, a feature matrix was constructed following Eq. (8). Note that for different vibration signals, the number of sensitive IMFs may differ. In a substantial experiment employing the correlation coefficient method, the largest number of sensitive IMFs was 6; i.e., m =6. The matrix of a vibration signal having fewer than six sensitive IMFs was filled with zero vectors.

After feature extraction, because of correlation and redundancy among the high-dimensional features, to improve the precision and efficiency of assessment, it is necessary to reduce the number of dimensions of the feature vector. This experiment compares the performance of four reduction algorithms, kernel principal component analysis (KPCA), LPP, local tangent space alignment (LTSA) and LLE algorithms. Three kernel functions are mainly used in the KPCA algorithm, namely the linear kernel function, the polynomial (Poly) kernel function and the radial basis kernel function (RBF). For these three kernel functions, the optimal parameters are sought using the grid-search method, each specified over a certain interval. The relationship between each parameter and the classification precision are then obtained, specified over reduced dimension d from 1 to 45, polynomial order q from 1 to 10, kernel width s of the RBF kernel function from 1 to 30. The experiment results are shown in Fig. 5.

The problem also is the selection of the reduced dimension number d and the number of neighboring points K in manifold learning. It is important that an appropriate number of parameters is considered. When the reduced dimension number is too large, the results will contain redundant information and the computational cost will be high. Conversely, the manifold in the low-dimensional space may create an overlap, resulting in the loss of discriminatory information. When the number of neighboring points K is too large, the algorithm cannot describe the local characteristics, and conversely, when the number is too high, it is not possible to maintain the topology structure between the sample points and neighboring points. This experiment selects parameters according to the classification precision of the SVM. Supposing that the classification precision is a function of parameters d and K, the function relation is $f = f(d, K)$. The aim is to find the optimal parameters d and K of the manifold algorithm with the maximum classification precision. The number of neighboring points K cannot be too small. The search area of K is from 3 to 45, where d ranges from 1 to 45; because the parameters must be integers, the step is set as 1. The SVM is the classifier, and the parameter selection results for each manifold algorithm are shown in Figs. 6–8.

From Fig. 5, it can be shown that, when RBF kernel function is selected in the KPCA algorithm and the kernel width s=22.9, reduced dimension number d=4, the classification precision will be the highest and reaches 89.17%. Figs. 6–8 show that when K=26 and d=2, the classification precision of the LPP algorithm is highest, reaching 80.27%, that when K=4 and d=1, the classification

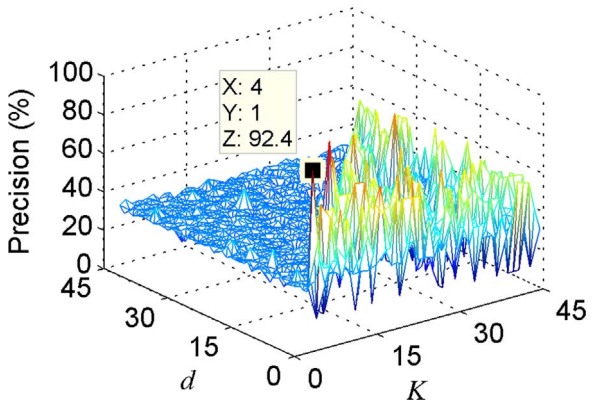

Fig. 7. Relations between the recognition precision and parameters d and K for LTSA.

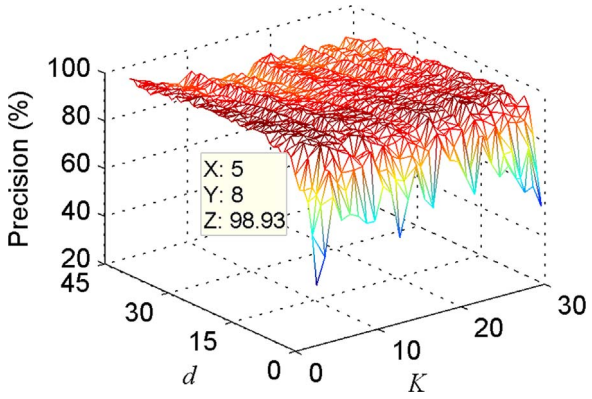

Fig. 8. Relations between the recognition precision and parameters d and K for LLE.

precision of the LTSA algorithm is highest, reaching 92.4%, and that when K=5 and d=8, the classification precision of the LLE algorithm is highest, exceeding 98%. Table 3 gives the classification precision of whether to reduce the number of dimensions of feature vectors, and whether to optimize the SVM parameters C and s. KPCA does not have the parameter of neighboring points, and therefore, to compare KPCA with other reduction algorithms, its reduced number of dimensions is set as the maximum d of the other three algorithms.

Table 3 shows that the classification precision of LPP without parameter optimization is only 80.27%, and without the dimension reduction is 86.53%. The classification precisions of KPCA, LTSA and LLE algorithm are higher than 86.53%, with LLE having the highest precision. After optimizing the parameters of the SVM, the classification precision without dimension reduction improves to 93.57%, the classification precisions of LPP, LTSA and LLE algorithms exceed 95%, and that of KPCA reaches 89.17%. The results show that the reduction algorithm eliminates redundant information in high-dimensional features. Compared with the case for unoptimized SVM parameters, there is a 10% improvement in the classification precision of LPP and LTSA. Additionally, LPP and LTSA make great demands of SVM parameters. The classification precision of LLE is highest in all cases, reaching about 99% after optimization of the parameters of the SVM.

In experimental scheme 1, training and testing data sets both contain vibration signals of the same rotational speed and load. To further verify the reliability of the proposed method, in a comparison with the data sets of experiment scheme 2, the classification precisions before and after reduction for different reduction methods are shown in Table 4. Also, the reduction method parameters and the optimal SVM parameters are presented. Obviously, for experimental scheme 2, a higher classification precision still can be obtained after feature reduction and SVM parameter optimization, and the LLE reduction algorithm still achieves the highest classification precision.

(2) Comparison of the time required for feature reduction.

The time required to run the four algorithms (KPCA, LPP, LTSA, LLE) for the same data is compared. The data sets consist of different fault locations of the bearing. The test results based on the data set of experiment scheme 1 are shown in Fig. 9.

Fig. 9 shows that the time required by the LTSA is the shortest, the time required by the LPP is longer than that required by the LTSA, and the time required by the KPCA is the longest, because the KPCA involves nonlinear mapping with a kernel function, which needs more computation. The KPCA is thus appropriate for real-time diagnosis. The average time required by the LLE is about 0.45 s, which is not much longer than that required by the LPP or LTSA.

A similar conclusion is drawn from an investigation of different performance degradation degrees of the rolling bearing. In the classification processing of the inner ring, rolling element and outer ring, the classification precision of LLE is about 4% points higher than that of KPCA, LPP and LTSA, on average. The present paper reduces the number of dimensions of a high-dimensional feature with LLE to realize quick and exact fault diagnosis.

Experiment 2: Experiment on the rolling-bearing state assessment model.

(1) Degradation relations of different fault locations and different fault degrees

Table 3
Comparison of recognition results before and after reduction for different reduction methods (Experiment scheme 1).

		KPCA	LPP	LTSA	LLE	No reduction
Manifold parameters	K	–	26	4	8	–
	d	4	2	1	5	–
Classification precision (%)		89.17	80.27	92.40	**98.93**	**86.53**
Optimized SVM parameters	C	36.54	89.71	36.42	34.41	34.67
	s	79.44	129.57	263.43	27.42	12.64
Optimized classification precision (%)		**92.86**	97.46	98.28	**99.40**	93.57

Table 4
Comparison of recognition results before and after reduction for different reduction methods (Experiment scheme 2).

		KPCA	LPP	LTSA	LLE	No reduction
Manifold parameters	K	–	28	5	7	–
	d	5	3	2	4	–
Classification precision (%)		75.43	71.65	78.35	**82.00**	**69.85**
Optimized SVM parameters	C	42.46	0.36	7.35	12.20	0.83
	s	88.93	144.36	338.29	225.64	514.27
Optimized classification precision (%)		88.43	82.56	85.62	**91.00**	81.23

Under the situation of the same fault degree at different fault locations, the relative distances between the normal state and three kinds of fault locations (i.e., inner ring, rolling element and outer ring) are compared. Based on the data set of experiment scheme 1, the relative distance d_R is calculated using Eq. (17). The relative distances of fault degrees 1, 2 and 3 for different fault locations are shown in Fig. 10a, b, and c. Because the data were normalized during the feature extraction and dimensional reduction procedures, the relative distances calculated subsequently are all dimensionless.

Fig. 10 shows a degradation relation for the same fault degree at different fault locations. The relationship conforms to the vibration propagation mechanism. In the course of propagation of the vibration signal, there is a certain vibration loss when the signal passes through other media. For the rolling bearing vibration signal, the relative distance between the normal state and the inner-ring fault is always larger than that for the rolling element at the same fault degree, with the rolling element larger than the outer ring. The relative distance relations among the different fault locations of the rolling bearing are verified.

Similarly, calculating the relative distances between the different fault degrees of the same fault location (inner ring, rolling elements, outer ring) and normal condition, and similar performance degradation relation can be obtained, with the relative distance decreasing as the fault degree increases, showing well the relationship between the different performance degradations.

(2) Assessment of different fault locations and different performance degradation states

Based on the data set of experiment scheme 1, the relative distances between the different fault locations and normal condition are compensated with Eq. (18) to obtain the relative compensation distances of different fault locations and performance degradation in the rolling bearing. The relative compensation distance is given in Table 5. The relative distances and relative compensation distance curves of several samples are shown in Fig. 11.

Fig. 11 shows that before compensating the relative distance of each fault location, the relative distances of different fault locations may overlap and may be similar. In this case, it is not possible to assess the running state of the rolling bearing. After compensating the relative distance of each fault location, there are clearly nine fault states, and a ladder configuration is observed. The configuration makes it convenient to find the relations between the relative compensation distance and fault states, and to make a visual assessment. According to the calculated relative compensation distance of each fault location, the threshold value between the inner-ring fault and rolling-element fault is about 0.255, while that between the rolling-element fault and outer-ring fault is about 0.07.

Based on the data sets of experiment scheme 2, the relative distance and the relative compensation distance of rolling bearing different fault state are shown in Fig. 12.

Fig. 12 shows that the obtained distance curves are similar to those in Fig. 11, but the load and rotational speed configuration of the test data sets in experiment scheme 2 are completely different from the training data sets. Hence, the degree of discrimination for each rolling bearing state in Fig. 12 is slightly worse than that in Fig. 11, which also can bee seen from the classification precision in Table 3. But, there are clearly nine fault states, and in general a ladder configuration is observed that conveniently assists the expert

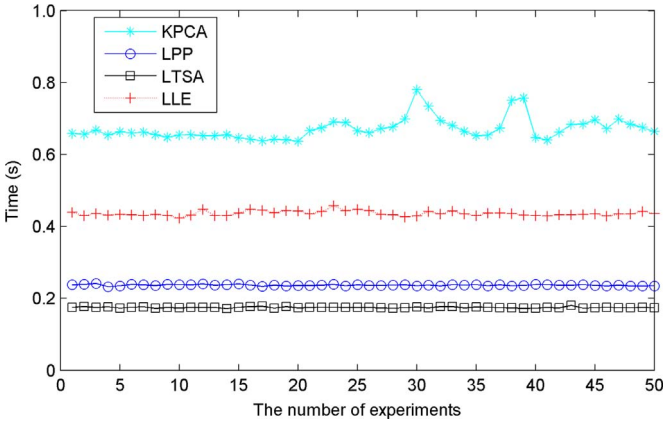

Fig. 9. Time required to run the four algorithms.

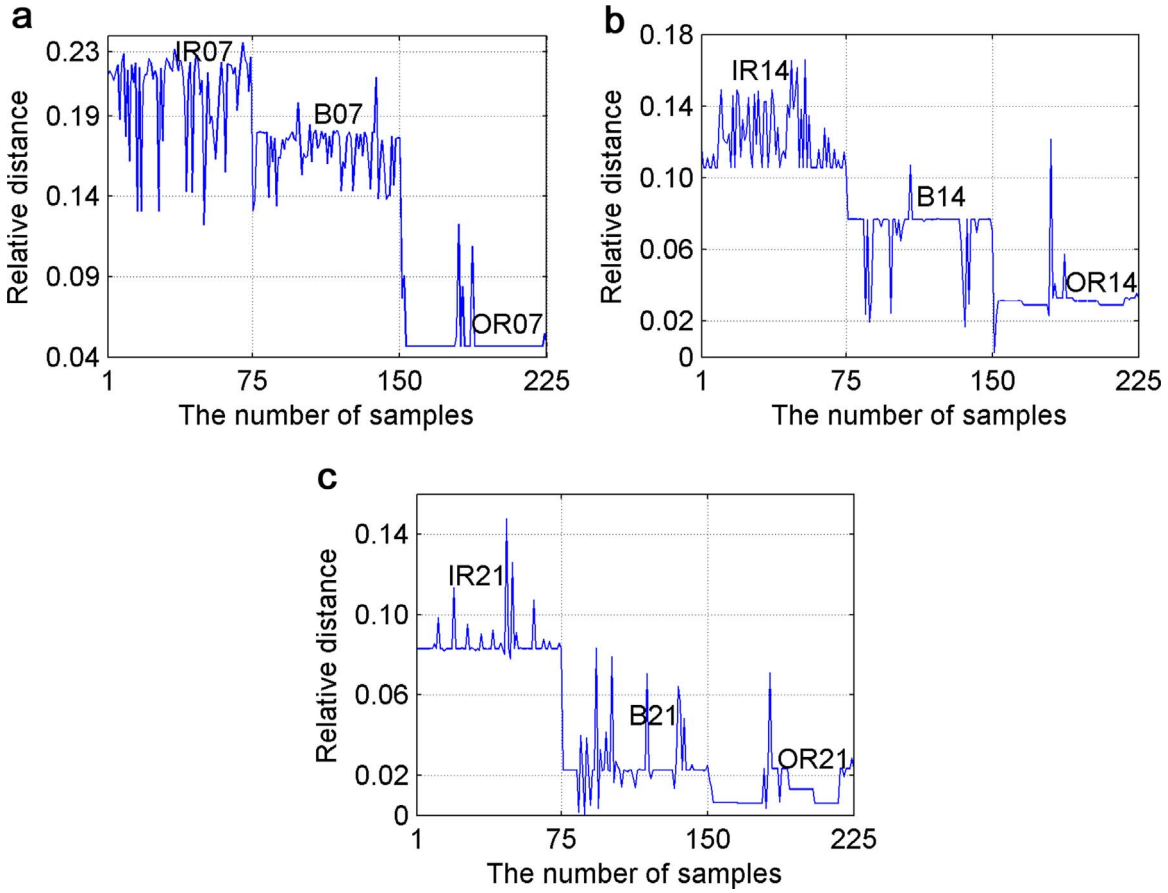

Fig. 10. The relative distances curve of different fault locations under different fault degrees: (a) fault degree 1, (b) fault degree 2, (c) fault degree 3.

to make a visual assessment.

To truly realize the assessment of different fault locations and different degrees of performance degradation for the rolling bearing, it is necessary to know the location of the current degradation state in the degradation curve, and the differences to the last state and next state. These differences are relative to the performance degradation degree of a rolling bearing, so as to realize an effective assessment of the rolling-bearing state. Singular points are eliminated in the distance curve drawn as a black line in Fig. 11. The mean of each stage of the distance curve is calculated, and the eight points that are farthest from the mean are then eliminated. The mean of each stage distance except for the singular points is then calculated. The data are then fitted with a quadratic function to get three smooth curves, namely the performance degradation assessment curve, as shown in Fig. 13. The performance degradation assessment curve based on the data sets of experiment scheme 2 are shown in Fig. 14.

Fig. 13 shows that the performance degradation assessment curve fitted by a quadratic function has a trend of decreasing monotonously. The trend of the relative compensation distance from large to small is the inner-ring fault, rolling-element fault and outer-ring fault. The fault degree is inversely proportional to the relative compensation distance. Additionally, the assessment value of the outer-ring fault is below 0.07 in the assessment curve, that of the rolling-element fault ranges from 0.07 to 0.255, and that of the inner-ring fault exceeds 0.255. The different locations within each range represent the different performance degradation of the rolling bearing. In testing the performance of the assessment model and index, first, the fault location is recognized. If the rolling bearing is in a normal state, the result ‘the rolling bearing is in a normal state’ is directly output. If the rolling bearing is not in a

Table 5
Typical relative compensation distance for each fault condition of the rolling bearing.

	IR07	IR14	IR21	B07	B14	B21	OR07	OR14	OR21
RCD of sample 1	0.38	0.30	0.27	0.23	0.13	0.08	0.05	0.03	0.01
RCD of sample 2	0.41	0.29	0.26	0.24	0.12	0.10	0.05	0.03	0.01
RCD of sample 3	0.36	0.33	0.29	0.24	0.12	0.08	0.05	0.03	0.01
RCD of sample 4	0.40	0.30	0.26	0.23	0.13	0.09	0.05	0.03	0.01
RCD of sample 5	0.37	0.29	0.26	0.20	0.12	0.10	0.05	0.03	0.01

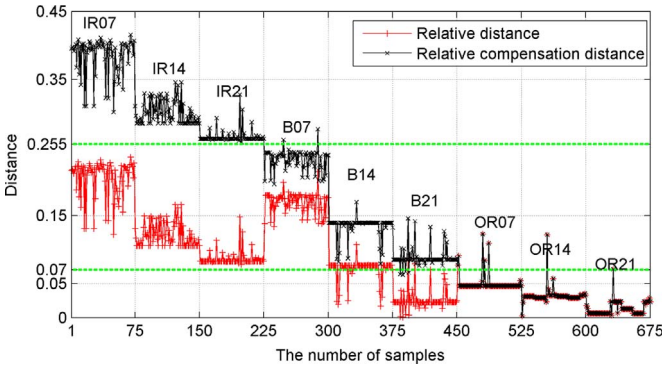

Fig. 11. Distance curves of different fault locations and performance degradation conditions (Experiment scheme 1).

normal state, the compensation distance is determined according to Eq. (18). The relative distance and compensation distance are then calculated, and a comparison is made with the performance degradation assessment curve to determine the degree of performance degradation of the rolling bearing. Similar judgments can be made from Fig. 14. Note that the corresponding trained assessment model and the assessment curve should be used when assessing actual vibration data.

(3) Assessment performance testing experiment

The classification precision of SVM model is a key factor that affects the precision of the assessment model. The above experiments have verified that the constructed classification model is precise and reliable. Based on the data set of experiment scheme 1, 50% of the sample data was randomly selected and tested to verify the performance of the constructed assessment model. The relative distance of each sample was calculated according to the SVM classification results, and the relative compensation distance was obtained by compensating the relative distance. Then the relative compensation distance were correlated with the corresponding position of the assessment curve. The assessment result of different fault locations and different performance degradation degrees of the rolling bearing is then obtained. Compared with the actual fault location and degradation state of the test samples, the assessment precision is calculated to be 93.93%. Based on the data sets of experiment scheme 2, the performance of the constructed assessment model is evaluated using the testing data sets B and D (data sets B and D account for 50% of the total data); the assessment precision is 89.74%. The experimental results of the classification precision and assessment precision for experiment schemes 1 and 2 are shown in Fig. 15.

Fig. 15 shows that, if the features obtained after LLE dimension reduction are used in the classification, the classification precisions of experiment schemes 1 and 2 are all higher than that without dimension reduction. Also, the classification precision obtained after optimizing SVM parameters using GA is higher than that without optimization. The precision obtained for experiment scheme 2 are all lower than that for experiment scheme 1, because the load and speed configuration of the testing data sets in experiment scheme 2 is completely different from the training data sets. For the two experiment schemes, the assessment precision is slightly lower than classification precision, but only the known fault locations and fault degrees of the training model can be classified. The assessment method based on the “relative compensation distance” not only can achieve the above classification, but also can simultaneously assess the fault locations and fault degrees that were not included in the training model. For example, if there is a bearing fault degree aside from 7 mil, 14 mil, and 21 mil, the proposed assessment method also can assess the fault degree and its fault location.

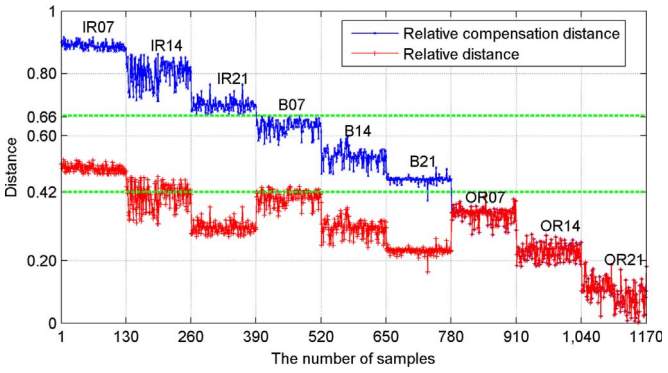

Fig. 12. Distance curves of different fault locations and performance degradation conditions (Experiment scheme 2).

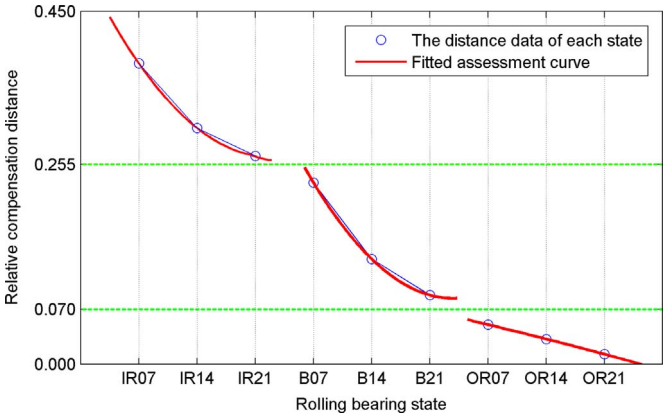

Fig. 13. Performance degradation assessment curve of the rolling bearing based on the SVM relative compensation distance (Experiment scheme 1).

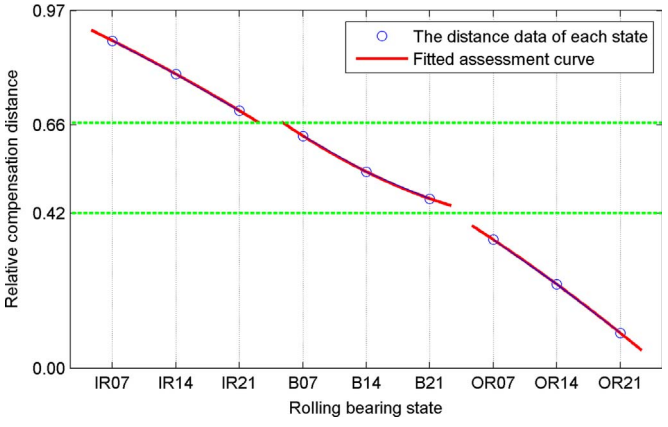

Fig. 14. Performance degradation assessment curve of the rolling bearing based on the SVM relative compensation distance (Experiment scheme 2).

6. Conclusion

In attempting to construct a common assessment index with which to assess the performance degradations resulting from faults at different locations, the present study proposed a novel method of assessing the state of a rolling bearing based on the relative compensation distance of multiple-domain features and employing a locally linear embedding. The study contributes with the following.

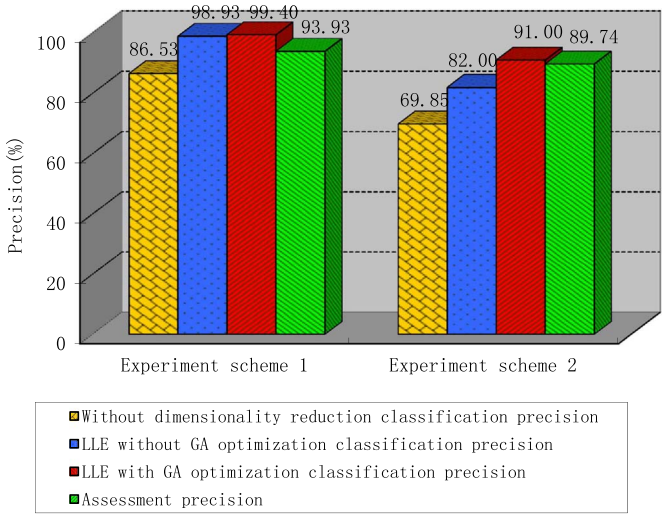

Fig. 15. Classification and assessment results of experiment schemes 1 and 2.

(1) To characterize the running state of a rolling bearing and to completely reflect the global and local characteristics of the vibration signal of the rolling bearing, we investigated a multiple-domain feature extraction method for the time domain, frequency domain and time–frequency features. The sensitive IMFs of improved EEMD with SVD were combined to extract the time–frequency features. Combining the time–frequency features with the time-domain and frequency-domain features of the original vibration signal and each sensitive IMF, we constructed a multiple-domain feature vector, which contains a complete set of characteristic information.
(2) The hybrid-domain feature reduction results of four feature reduction algorithms—KPCA, LLE, LPP and LTSA—were compared according to the manifold structure of rolling-bearing feature data. The LLE algorithm is suitable for feature reduction, and can effectively eliminate redundancy among high-dimensional feature vectors, improve the classification precision of rolling-bearing fault diagnosis, and save time for the subsequent assessment.
(3) According to the theory of the SVM, we proposed an assessment method based on 'relative distance'. The method is effective in assessing different fault degrees for the same fault location, but ineffective in assessing different fault locations and different degrees of performance degradation overall. Considering the structure, fault location and vibration transmission mechanism of the rolling bearing, we proposed a novel multiple-state assessment model for the rolling bearing. Experimental results show that the model can assess different fault locations and different degrees of performance degradation at the same time, demonstrating the effectiveness of the proposed assessment method under certain conditions.

In addition, the proposed method should be further verified using vibration data from a rolling bearing obtained from actual equipment. Moreover, the effectiveness of the relative compensation distance scheme needs further study for situations when the sensor cannot be situated near the outer ring of the bearing and when a different type of bearing is used as a replacement.

Acknowledgments

This work was supported by the National Natural Science Foundation of China (Grant No. 51305109), the Natural Science Foundation of Heilongjiang Province (Grant No. QC2014C075), and the Hei Long Jiang Postdoctoral Foundation (Grant No. LBH-Z13113), and Program for the Top Young Innovative Talents of Harbin University of Science and Technology (Grant No. 11).

Appendix A. Supporting information

Supplementary data associated with this article can be found in the online version at doi:10.1016/j.ymssp.2016.10.006.

References

[1] Pavle Boškoski, Matej Gašperin, Dejan Petelin, Đani Juričić, Bearing fault prognostics using Rényi entropy based features and Gaussian process models, Mech. Syst. Signal Process. 52–53 (2015) 327–337.
[2] Robert B. Randall, J.érôme Antoni, Rolling element bearing diagnostics—a tutorial, Mech. Syst. Signal Process. 25 (2011) 485–520.
[3] Jaouher Ben Ali, Nader Fnaiech, Lotfi Saidi, Brigitte Chebel-Morello, Farhat Fnaiech, Application of empirical mode decomposition and artificial neural network for automatic bearing fault diagnosis based on vibration signals, Appl. Acoust. 89 (2015) 16–27.
[4] F. Jia, Y.G. Lei, J. Lin, X. Zhou, N. Lu, Deep neural networks: a promising tool for fault characteristic mining and intelligent diagnosis of rotating machinery with massive data, Mech. Syst. Signal Process. (2016) 303–315.
[5] Jaouher Ben Ali, Brigitte Chebel-Morello, Lotfi Saidi, Simon Malinowski, Farhat Fnaiech, Accurate bearing remaining useful life prediction based on Weibull distribution and artificial neural network, Mech. Syst. Signal Process. (2015) 150–172.
[6] H.M. Jiang, J. Chen, G.M. Dong, T. Liu, G. Chen, Study on Hankel matrix-based SVD and its application in rolling element bearing fault diagnosis, Mech. Syst. Signal Process. (2015) 338–359.
[7] L. Zhang, W.Y. Huang, G.L. Xiong, J.M. Zhou, J.H. Zhou, Bearing performance degradation assessment based on TESPAR and GMM, Chin. J. Sci. Inst. 35 (8) (2014) 1772–1779.
[8] Wei He, Qiang Miao, Michael Azarian, Michael Pecht, Health monitoring of cooling fan bearings based on wavelet filter, Mech. Syst. Signal Process. (2015) 149–161.
[9] Y.X. Huang, C.L. Liu, X.F. Zha, Y.M. Li, A lean model for performance assessment of machinery using second generation wavelet packet transform and Fisher criterion, Exp. Syst. Appl 37 (5) (2010) 3815–3822.
[10] Y.G. Lei, Z.J. He, Y.Y. Zi, Q. Hu, Fault diagnosis of rotating machinery based on multiple ANFIS combination with Gas, Mech. Syst. Signal Process. 21 (2007) 2280–2294.
[11] K.M. Qian, A simple phase unwrapping approach based on filtering by windowed Fourier transform: a note on the threshold selection, Opt. Laser Technol. 40 (8) (2008) 1091–1098.
[12] Q. Guo, P.Y. Liu, L.B. Shi, B. Li, Experimental study and fault signals analysis of rotating machinery based on dual EEMD and wigner-ville distribution, J. Vib. Shock 31 (13) (2012) 129–133 [153].
[13] H.X. Li, Bearing fault diagnosis based on wavelet analysis, Adv. Mater. Res. (2013) 1763–1768.
[14] N.E. Huang, Z. Shen, S.R. Long, The empirical mode decomposition and the Hilbert spectrum for nonlinear and non-stationary time series analysis, Proc. R. Soc. Lond. Ser. 454 (1998) 903–995.
[15] Z. WU, N.E. Huang, Ensemble empirical mode decomposition: a noise assisted data analysis method, Data Anal. 1 (2009) 1–41.
[16] Y.J. Wang, Y.C. Jiang, S.Q. Kang, G.X. Yang, Y.N. Chen, Diagnosis method of fault location and performance degradation degree of rolling bearing based on optimal ensemble EMD, Chin. J. Sci. Instrum. 34 (8) (2013) 1834–1840.
[17] L. Lin, L. Yu, Improvement on empirical mode decomposition based on correlation coefficient, Comput. Digit. Eng. 36 (12) (2008) 28–36.
[18] Z.K. Peng, P.W. Tse, F.L. Chu, A comparison study of improved Hilbert-Huang transform and wavelet transform: application to fault diagnosis for rolling bearing, Mech. Syst. Signal Process. 19 (5) (2005) 974–988.
[19] B. Zhang, L.J. Zhang, J.W. Xu, P.F. Wang, Performance degradation assessment of rolling element bearings based on an index combining SVD and information exergy, Entropy 16 (2014) 5400–5415.
[20] J.B. Yu, Bearing performance degradation assessment using locality preserving projections and Gaussian mixture models, Mech. Syst. Signal Process. 25 (7) (2011) 2573–2588.

[21] T. Benkedjouh, K. Medjaher, N. Zerhouni, S. Rechak, Remaining useful life estimation based on nonlinear feature reduction and support vector regression, Eng. Appl. Artif. Intell. 26 (7) (2013) 1751–1760.
[22] E.P. De Moura, C.R. Souto, A.A. Silva, M.A.S. Irmão, Evaluation of principal component analysis and neural network performance for bearing fault diagnosis from vibration signal processed by RS and DF analyses, Mech. Syst. Signal Process. 25 (5) (2011) 1765–1772.
[23] B.W. Li, Y. Zhang, Supervised locally linear embedding projection for machinery fault diagnosis, Mech. Syst. Signal Process. 25 (8) (2011) 3125–3134.
[24] S.Q. Kang, Z.Q. Li, G.X. Yang, Y.J. Wang, Application of wavelet packet -locally linear embedding algorithm in rolling bearing fault degree recognization, Chin. J. Sci. Instrum. 35 (3) (2014) 614–619.
[25] Lotfi Saidi, Jaouher Ben Ali, Farhat Fnaiech, Application of higher order spectral features and support vector machines for bearing faults classification, ISA Trans. 54 (2015) 193–206.
[26] J.T. Huang, M.H. Wang, K.K. Xu, Rolling bearing fault diagnosis fusion model based on gene expression programming, J. Inf. Comput. Sci. 7 (12) (2010) 2437–2442.
[27] H.B. Yang, Features extraction and selection in rolling bearing fault diagnosis, Hunan University of Technology, Hunan, 2011, pp. 68–77.
[28] K.A LoparoBearings vibration data set, Case Western Reserve University [EB/OL] ⟨http://www.eecs.case.edu/laboratory/bearing/welcome_overview.htm⟩.